RESEARCH ARTICLE

Computational Neuroscience

Ramping dynamics in the frontal cortex unfold over multiple timescales during motor planning

Rifqi O. Affan,[1] Ian M. Bright,[2] Luke N. Pemberton,[2] Nathanael A. Cruzado,[2] Benjamin B. Scott,[2] and Marc W. Howard[2]

[1]Graduate Program in Neuroscience, Boston University, Boston, Massachusetts, United States and [2]Department of Psychological and Brain Sciences, Boston University, Boston, Massachusetts, United States

Abstract

Plans are formulated and refined throughout the period leading up to their execution, ensuring that the appropriate behaviors are enacted at the appropriate times. Although existing evidence suggests that memory circuits convey the passage of time through diverse neuronal responses, it remains unclear whether the neural circuits involved in planning exhibit analogous temporal dynamics. Using publicly available data, we analyzed how activity in the mouse frontal motor cortex evolves during motor planning. Individual neurons exhibited diverse ramping activity throughout a delay interval that preceded a planned movement. The collective activity of these neurons was useful for making temporal predictions that became increasingly precise as the movement time approached. This temporal diversity gave rise to a spectrum of encoding patterns, ranging from stable to dynamic representations of the upcoming movement. Our results indicate that ramping activity unfolds over multiple timescales during motor planning, suggesting a shared mechanism in the brain for processing temporal information related to both memories from the past and plans for the future.

NEW & NOTEWORTHY Neuronal responses in the cortex are diverse, but the nature and functional consequences of this diversity remain ambiguous. We identified a specific pattern of temporal heterogeneity in the mouse frontal motor cortex, whereby the firing of different neurons ramps up at varying speeds before the execution of a movement. Our decoding analyses reveal that this heterogeneity in ramping dynamics enables precise and reliable encoding of movement plans and time across various timescales.

frontal cortex; motor planning; neuronal heterogeneity; ramping activity; time

INTRODUCTION

Adaptive behavior requires certain actions to be executed at precisely the right moments. Humans and other animals often accomplish this by anticipating upcoming events and preparing actions in advance. Effective motor planning involves not only this prospection but also the flexibility to make continuous adjustments, while gradually increasing commitment as the moment of action approaches. These computational considerations suggest an underlying neural system for motor planning that is capable of tracking the progression of time.

The challenge of anticipating when an action should be taken in the future is analogous to the problem of estimating when an event was encountered in the past. In the hippocampus, neurons described as "time cells" (1–3) fire transiently at different moments following the presentation of a stimulus, forming distinct sequences that tile the intervals that follow different events (4, 5). In contrast, "temporal context cells" in the entorhinal cortex activate immediately in response to a stimulus and then gradually relax to baseline with a variety of time constants (6, 7), conveying time elapsed since the stimulus across multiple timescales. Whether these temporal dynamics are exclusive to parts of the brain that are involved in memory or whether they are more broadly reflected across the cortex for the prospective control of actions remains unclear.

The anterior lateral motor (ALM) cortex is a key brain structure involved in motor planning in mice (8–11). Many neurons in the ALM display firing rates that gradually increase or decrease during a delay interval that precedes the execution of a planned movement, a pattern commonly

referred to as ramping activity ([11], [12]). Although ramping activity in the ALM has generally been examined at the population level ([13]–[16]), often using dimensionality reduction to summarize heterogeneous activity patterns across neurons, less focus has been placed on assessing the heterogeneity within the population of neurons. In this study, we use a publicly available dataset ([12], [17]) to evaluate the variability in ramping dynamics across ALM neurons. We show that ramping activity in the ALM is characterized by a distribution of ramping time constants. We assess and discuss the potential implications of this temporal heterogeneity for the encoding of time and motor plans in the ALM cortex.

MATERIALS AND METHODS

Data Description

To evaluate the temporal heterogeneity of ramping activity across frontal cortical neurons during motor planning, we analyzed data previously reported by Inagaki et al. ([12]). The data were retrieved on May 15, 2020, from the publicly available database CRCNS (https://crcns.org/data-sets/motor-cortex/alm-5/about-alm-5).

Behavioral Paradigm

Inagaki et al. ([17]) provided data collected from head-fixed mice engaged in an auditory-based, fixed delay task. Each trial in the task began with a series of 150 ms tones with 100 ms between each tone. The tones were either 3 or 12 kHz. This sampling period lasted 1.15 s and was immediately followed by a 2 s delay period. The delay period ended with a 100 ms auditory go cue (6-kHz carrier frequency with 360-Hz modulating frequency). The go cue indicated mice to lick the right lick-port if they were presented with 3 kHz tones during the sampling period, or the left port if they were presented with 12 kHz tones. Mice were rewarded 2 µL of water if they licked the correct side within a 1.5 s response period following the go cue. Only trials when the animal correctly responded were included in the current paper.

Electrophysiological Data

The dataset included processed spike trains of 755 single units that were recorded by Inagaki et al. ([12]) from the left ALM cortex of six mice across 20 sessions of auditory-based fixed delay task. Details of the recording and spike-sorting procedure are described by the authors of the original report. An example MATLAB code was provided by Inagaki et al. ([12], [17]) as part of the archived data in CRCNS to access the time stamps of spike events across the trials of each session. The authors of the original paper labeled 667 of the 755 single units as putative pyramidal neurons based on the width of their spike waveform. The procedure for identifying putative pyramidal neurons is described in detail in the original paper ([12]). Only spike trains of the putative pyramidal neurons were analyzed in the current paper. The dataset also includes trials in which spikes were recorded during simultaneous photoinhibition, but we excluded these trials from the analyses in the current paper.

Delay Activity and Trial-Type Selectivity

We used the same approach as by Inagaki et al. ([12]) to identify putative pyramidal neurons that show significant upward and downward ramping activity. A Mann–Whitney U test revealed that 516 of the 667 putative pyramidal neurons showed a significant difference between firing rate estimated within the 1 s interval before trial onset and firing rate estimated within the 2 s delay interval. Some of these neurons ramp up in firing during the delay ($n = 302/516$) while others ramp down ($n = 214/516$).

We estimated a normalized selectivity score for the delay activity of each neuron following the protocol used by Inagaki et al. ([12], [17]):

$$\text{Selectivity} = \frac{(\text{FR}_\text{R} - \text{FR}_\text{L})}{\text{FR}_\text{R} + \text{FR}_\text{L}} \quad (1)$$

where FR_R is the average firing rate (spikes/s) during the delay period across correct right-lick trials and FR_L is the average firing rate (spikes/s) during the delay period across correct left-lick trials. The selectivity score ranges from −1 to 1. A positive selectivity value indicates that a neuron is more responsive during the right-lick trials and a negative value indicates that a neuron is more responsive during the left-lick trials. We used a Wilcoxon rank-sum test to test whether the firing rate of each neuron is different between right- and left-lick trials. The results were used to determine whether each neuron is trial-type selective.

Temporal Receptive Field Models

To quantify the time course of activity for each neuron in the ALM cortex, we adapted an analysis method used to identify and characterize time-varying signals across monotonically firing neurons in the monkey entorhinal cortex ([7]) and stimulus-specific time cells in the monkey hippocampus and prefrontal cortex ([18]). For this analysis, temporal receptive field models were fit to the spikes of 516 putative pyramidal neurons within a 3.15 s interval preceding a Go cue, starting from the onset of the 1.15 s stimulus presentation period ($t = -3.15$ s relative to Go cue) to the end of the 2 s delay period ($t = 0$ s relative to Go cue). We considered three receptive field models: 1) a constant firing model, 2) a ramping ex-Gaussian model, and 3) a ramping ex-Gaussian model with trial-type specificity. Neurons that were identified as nonselective were fit by the second model, whereas those labeled as selective were fit by the third model.

The constant model consisted of a single parameter a_0 that predicted the constant probability of a spike at each time t:

$$M_{\text{const}}(t; a_0) = a_0 \quad (2)$$

The ramping ex-Gaussian model defines the temporal modulation of the firing field as the convolution of the Gaussian function and an exponentially ramping function. The classical ex-Gaussian model can be numerically expressed as:

$$M_{\text{exG}}(t; a_0, a_1, \sigma, \mu, \tau) = a_0 + \frac{a_1}{2} e^{\frac{\left(2\mu + \frac{\sigma^2}{\tau} - 2t\right)}{2\tau}} erfc\left(\frac{\mu + \frac{\sigma^2}{\tau} - t}{\sqrt{2}\sigma}\right) \quad (3)$$

Here, a_0 estimated the contribution of the constant baseline while a_1 estimated the contribution of the time-varying function. A downward ramp can be achieved by letting a_1 be negative. The Gaussian parameter μ defines the location of

peak response along the time axis while σ determines its variability. The parameter τ represents the time constant of the exponential decay function and is defined as the time that a neuron has decreased its firing 37% away from baseline. *erfc* is the complimentary error function. To capture a ramping dynamic that changes as a function of time until the target interval, we substituted t with T-t. Here, T is the total duration starting from the trial onset and ending with the go cue (3.15 s).

To account for response variability across different trial types (correct, right-lick vs. left-lick trials), the ramping ex-Gaussian model was extended by replacing a_1 from *Eq. 3* with two peak amplitude terms. a_1 estimated the contribution of the time term for right-lick trials while a_2 determined the contribution of left-lick trials. The full, trial-type specific ex-Gaussian model for the ramping time term can be numerically expressed as:

$$M_{\text{exG}}(t; a_0, a_1, \sigma, \mu, \tau) = a_0$$
$$+ \sum_{i=1}^{2} c_i \frac{a_i}{2} e^{\frac{\left(2\mu + \frac{\sigma^2}{\tau} - 2(T-t)\right)}{2(T-t)}} erfc\left(\frac{\mu + \frac{\sigma^2}{\tau} - (T-t)}{\sqrt{2}\sigma}\right) \quad (4)$$

Here, c_1 was set to equal 1 for right-lick trials and 0 otherwise while c_2 was set to equal 1 left-lick trials only.

We calculated the fit of the receptive field models to spikes across a total of 3,150 time bins (from the trial onset to the go cue) using a custom maximum likelihood estimation script run in MATLAB 2016a. The parameter μ was allowed to be any value between -1 s to 0 s (1 s preceding the Go cue) and σ was permitted to range between 0 and 0.30 s. The parameter τ was permitted to range between 0.01 and 5 s. The likelihood of the model fits was determined as a product of the probabilities of a spike across time bins within and across trials. We implemented the maximum likelihood parameter estimation using particle swarm (with the swarm size equal to 50). The fitting procedure was repeated until the algorithm failed to output higher likelihood for 20 consecutive iterations to avoid local minimum convergence.

We performed a goodness-of-fit test for each neuron by estimating the R^2 value of the ex-Gaussian model fit to the average firing rate within the 3.15 s interval preceding the Go cue. We use this approach to exclude neurons whose model fit failed to achieve an R^2 value of greater than 0.5.

Statistical Analyses

Unbiased estimates of skewness and Pearson's kurtosis were obtained for the distribution of time constant using the *descdist* function in *R* with the argument *boot* set to 1,000 for nonparametric bootstrapping. Maximum likelihood estimations were performed to fit uniform, normal, log-normal, and gamma distributions to time constant data using the *R* function *fitdist*. We reported the mean and standard error of parameter estimates for all distribution models. AIC and BIC estimates were used to compare the goodness-of-fit measures of these distribution models.

Pairwise Differences

To assess the presence of diversity in time constant within and between different sessions, we measured the absolute difference between pairs of time constant values corresponding to each neuron. In the pooled condition, pairwise differences were measured between all possible pairs of neurons. In the

within-session conditions, we measured time constant differences exclusively between pairs of neurons recorded within the same sessions. To measure differences in time constants across various recording sessions, we compared neurons belonging to different sessions from the same animals. These measurements were computed using a custom function in *R*.

Variance Component Analysis

To quantify the variance in time constant values τ attributable to differences between recording sessions and animals, we used a generalized linear mixed-effects model (GLMM). The GLMM is formulated as follows:

$$\tau_{ijk} = \beta_0 + u_{0i} + v_{0ij} + \epsilon_{ijk} \quad (5)$$

Here, τ_{ijk} represents the time constant for the i-th neuron in the k-th session of the j-th animal. The term β_0 is the fixed intercept, representing the overall mean time constant across all animals and sessions. The terms μ_{0i} and v_{0ij} are the random intercepts for each animal and each session within an animal, respectively, and ϵ_{0ij} is the residual error term. We assume the random effects are normally distributed with mean zero and variances σ^2_{animal} for animals and $\sigma^2_{\text{session} \mid \text{animal}}$ for sessions within animals. The residual variance σ^2_{ϵ} accounts for the unexplained variability in time constant. Given the right-skewed and heavy-tailed shape we observed for the distribution of time constant, we assumed τ to follow a gamma distribution in this GLMM. This model was implemented in R using the *glmer* function with the *family* argument set to *Gamma*. In addition, we applied a bootstrapping approach to estimate and report the variance components relative to the total variance.

LDA for Decoding Time

A linear discriminant analysis (LDA) classifier was used to decode time within the trial from the population activity of ramping neurons. The classifier was trained on even trials and tested on odd trials. We randomly sampled 125 trials for each neuron as the number of trials varied across neurons. Time within each trial was segmented into 100 ms bins. Firing rate across neurons were calculated for each bin of each trial. A uniform noise, ranging from 0 to 1×10^{-13} Hz, was inserted to the firing rate in each time bin to minimize errors due to a singular covariance matrix. The averaged firing rate of each time bin for each trial across all neurons provides a sample of the training and testing data. This analysis was implemented using the MATLAB function *classify.m* using "linear" as the specified discriminant type.

Cross-Temporal Decoding of Trial Type

To assess how movement direction, or the associated cue, is encoded by subpopulations of ramping neurons with different time constants, we trained and tested LDA classifiers to predict whether animals correctly licked left or right at every possible pair of time points throughout the trial interval (19–22). Each subpopulation of neurons comprised 72 neurons. The range of time constant τ associated with each subpopulation is described in the RESULTS. As the number of trials varied across neurons, we randomly sampled 125 trials for each neuron in slow-, medium-, and fast-ramping subpopulation I, II, and III. We segmented the 2 s delay intervals into 100 ms bins. We trained the classifiers on 80% of

the sampled trials and tested them on the remaining 20% of the trials for each pair of time bins. The firing activity across neurons was calculated for each bin of each trial. We used the MATLAB function *rref.m* to reduce the training data to full rank and identify the pivots before each run of the classifier. This was performed to ensure the stability of the LDA. The LDA classifier was then implemented using the MATLAB function *classify.m*. We repeated training and testing procedures for 20 iterations. To obtain robust results, we randomly sampled subsets of trials and 71 of 72 neurons in each subpopulation at each iteration. This procedure yielded an accuracy matrix for each of the three subpopulations. The matrix is composed of pairs of training and testing time bins. Identical training and testing time bins lie along the diagonal of this matrix. The off-diagonal values of the accuracy matrix indicate the similarity in how information is encoded by the population between two different time points.

Alternative and Independent Estimation of Time Constants

We used the Zeratti et al.'s (23) model to independently evaluate time constants for neurons designated as either ramp or decay. Their unbiased method uses a generative model to evaluate the time constants from the sample autocorrelation of an Ornstein–Uhlenbeck (OU) process as opposed to the biased method of fitting an exponential curve directly to the autocorrelation function of a time series. Using their *abcTau* python package, we fit a one tau OU process model and a two tau OU process model to the average firing rates of each neuron across a 3,150 ms interval preceding the Go cue. We then estimated the autocorrelation of each neuron with a bin size of 50 ms. For the one tau OU process, we assumed a uniform prior with the min $\tau = 0$ ms and max $\tau = 10,000$ ms. For the two tau OU process, we assumed the same distribution for τ_1 and a uniform prior with the min $\tau = 100$ ms and max $\tau = 10,000$ ms for τ_2, with $\tau_2 > \tau_1$ enforced. The prior coefficient or weight for the first timescale was uniform between 0 and 1. We used a linear distance function and model hyperparameters $\varepsilon_0 = 1$, min samples = 100, steps = 60, and minAccRate = 0.01. We then used the inbuilt model comparison *abcTau.compcdf()* module to calculate the Bayes factor between the two models for each cell. If the one tau OU model fits better that tau was taken as the timescale for that cell. Otherwise, τ_2 from the two tau OU process was taken as the timescale for that cell.

RESULTS

In this study, we assessed the temporal heterogeneity of ramping activity in the ALM cortex of mice during motor planning. We used a model-based approach (7, 18) to analyze an open-source dataset (12, 17) containing preprocessed extracellular recordings from the ALM cortex of mice performing a delayed response task. A schematic diagram of the task is illustrated in Fig. 1A. As previously reported by Inagaki et al. (12), many neurons in the ALM cortex showed firing rates that fluctuate during a 2 s long delay period before a motor response ($n = 516$ of 667 putative pyramidal units). Some neurons showed an increase in firing rate as time approaches the end of the delay period ($n = 302$ of 516 neurons), while others showed a decrease from baseline

firing ($n = 214$ of 516 neurons). Most neurons exhibited some level of selectivity in their firing for right- versus left-lick trials ($n = 344$ of 516 neurons) while others show no preference for one trial type over the other ($n = 172$ of 516 neurons). The firing rates of a few example neurons are shown in Fig. 1B. The diversity of selectivity and ramping direction in this dataset has been characterized in the original report (12). The primary focus of this paper is to evaluate whether motor preparatory ramps, as identified by Inagaki et al. (12), have a single homogeneous timescale or if the ramps show heterogeneous timescales across neurons during the delay period (Fig. 1C). Neurons that ramp downward are of secondary interest in this paper and are briefly reported in the end of the RESULTS and in the supplement.

Receptive Field Model Estimates the Temporal Properties of Single-Neuron Firing

To quantify the temporal characteristics of neural activity in the ALM cortex, we estimated their temporal receptive fields as a convolution of a Gaussian (latency of the activity) and an exponential ramp (Fig. 1D). Under this model, the latency of each neuron's activity is described by the mean of the Gaussian function μ. The rate at which each neuron's activity ramps up or down is described by the time constant of the exponential term τ. An additional parameter σ determines the standard deviation of the Gaussian function. We identified ramp-up versus ramp-down and selective versus nonselective neurons as determined in the original report of these data (12). Neurons that show trial-type selectivity were fit with two amplitude terms corresponding to right- versus left-lick trials. Neurons that show downward ramping of activity were fit with a negative amplitude term. Details of the parameter estimation procedure are described in MATERIALS AND METHODS.

Using this approach, we identified 216 upward ramping neurons in the ALM cortex whose firing activity was fit by the ex-Gaussian receptive field model with an R^2 value greater than 0.5 (Fig. 1E). These neurons make up 64.07% of the total 334 putative pyramidal neurons that were fit with $R^2 > 0.5$. Neurons with R^2 values less than 0.5 were excluded from further analysis.

Neural Activity in the ALM Cortex Evolves with Heterogeneous Time Constants

Different ALM neurons displayed firing rates that ramp up at varying speeds over the course of the 2 s delay interval. Slower ramping neurons, such as the three shown in the top row of Fig. 2A, began to change their firing rate as early as the stimulus period (between −3.15 s and −2 s to the Go cue) and gradually reached maximum or minimum firing rate around the Go cue. In contrast, faster ramping neurons, like those shown in the bottom row of Fig. 2A, displayed a more abrupt change in firing rate later in the delay period and reached maximum or minimum activity at the time of the Go cue. The variability in ramping dynamics across all 216 ALM neurons is displayed in Fig. 2B.

There was a wide range of time constants across neurons, as indicated by a median τ of 0.97 s and an interquartile range from 0.57 s to 1.74 s. Notably, 90% of the time constants were less than or equal to 3.42 s. Figure 2C shows the histogram and cumulative distribution of time constant
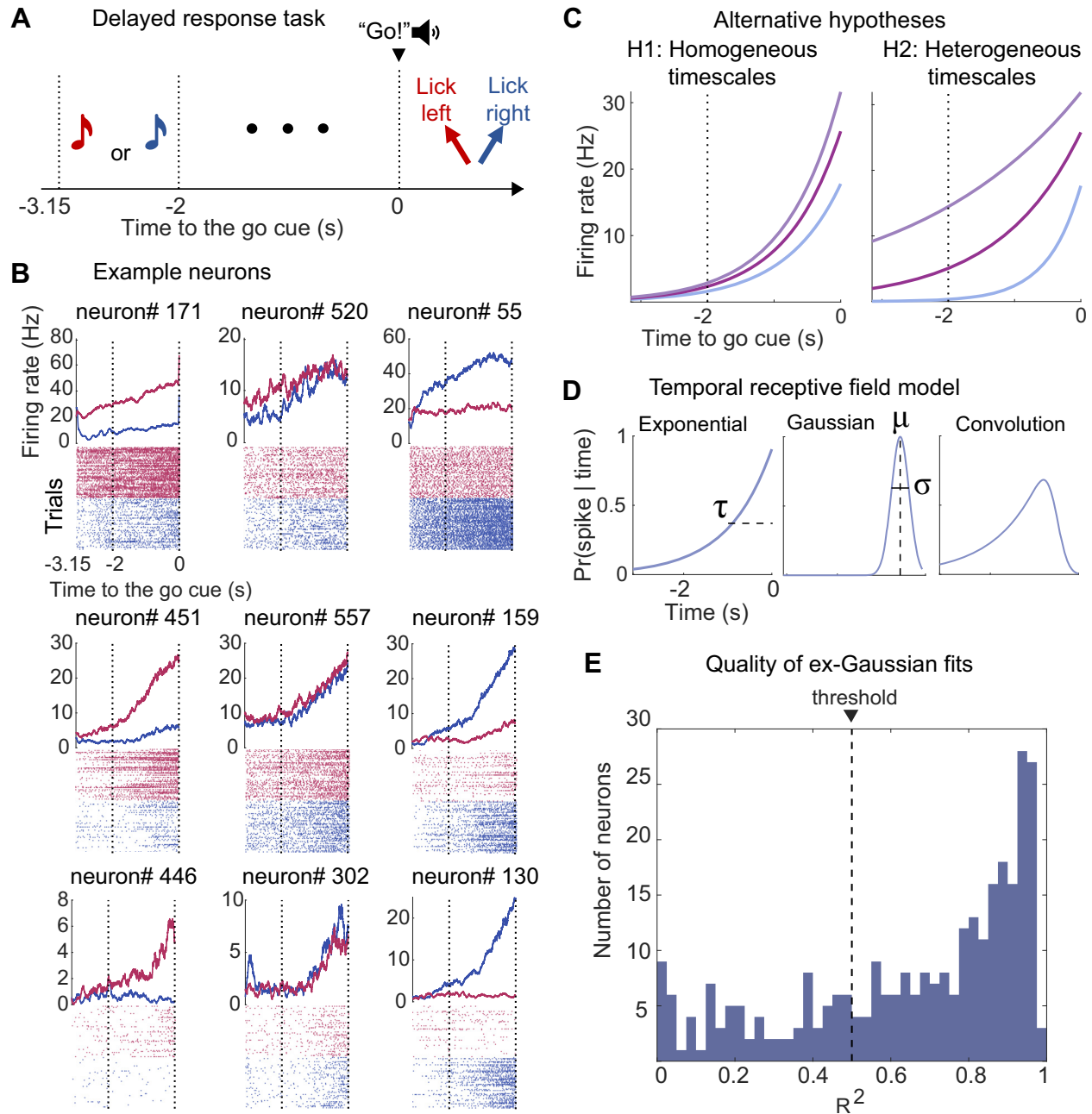
Figure 1. Schematic of the delayed response task and hypotheses for neural activity. *A*: auditory-delayed response task from Inagaki et al. ([12], [13], [17]). Red represents trials where mice are presented with high-pitch tones, instructing them to lick leftward following a Go cue. Blue corresponds to trials with low-pitch tones, instructing them to lick rightward. *B*: example neurons in the ALM cortex. *Top*: cross-trial average PSTHs. *Bottom*: spike raster plots of 50 randomly sampled trials for each condition. Error trials are excluded from the analyses. Vertical dotted line marks the start and end of the delay period. Some neurons selectively fire in one type of trial over the other (left column and right column), discriminating the direction of the future lick response. Some neurons gradually ramp up during the delay period (top row), while others ramp up more abruptly at the end of the delay period (bottom row). *C*: alternative hypotheses for temporal heterogeneity during motor planning. H1: individual neurons ramp over the delay period with similar time constants. H2: individual neurons ramp with different time constants. *D*: an ex-Gaussian receptive field model of neuron firing activity. The ex-Gaussian receptive field model (*right*) is generated from the convolution of an exponential function (*left*) and a Gaussian function (*middle*). This model describes neuronal response as a function of time with the time constant parameter τ, the peak latency parameter μ, and the parameter σ. *E*: quality of the model fit across ramping neurons. Most upward ramping neurons were fit by the ex-Gaussian model with $R^2 > 0.5$ (black dashed line). ALM, anterior lateral motor.

values, revealing a skewed distribution (skewness = 1.56) with a heavy tail (kurtosis = 4.64). The spread of time constants across neurons was best approximated by a gamma distribution with a shape parameter of 1.39 ± 0.12 (SE) and a rate parameter of 0.97 ± 0.10 (AIC = 575.55, BIC = 582.30), followed by a log-normal distribution with a location parameter

of -0.05 ± 0.07 (SE) and a scale parameter of 0.99 ± 0.05 (ΔAIC and ΔBIC = 17.39), a uniform distribution (ΔAIC and ΔBIC = 122.86), and a normal distribution with a mean of 1.42 ± 0.09 (SE) and a standard deviation of 1.29 ± 0.06 (ΔAIC and ΔBIC = 149.92). Together, these results imply that while most neurons exhibited shorter ramping time constants, a
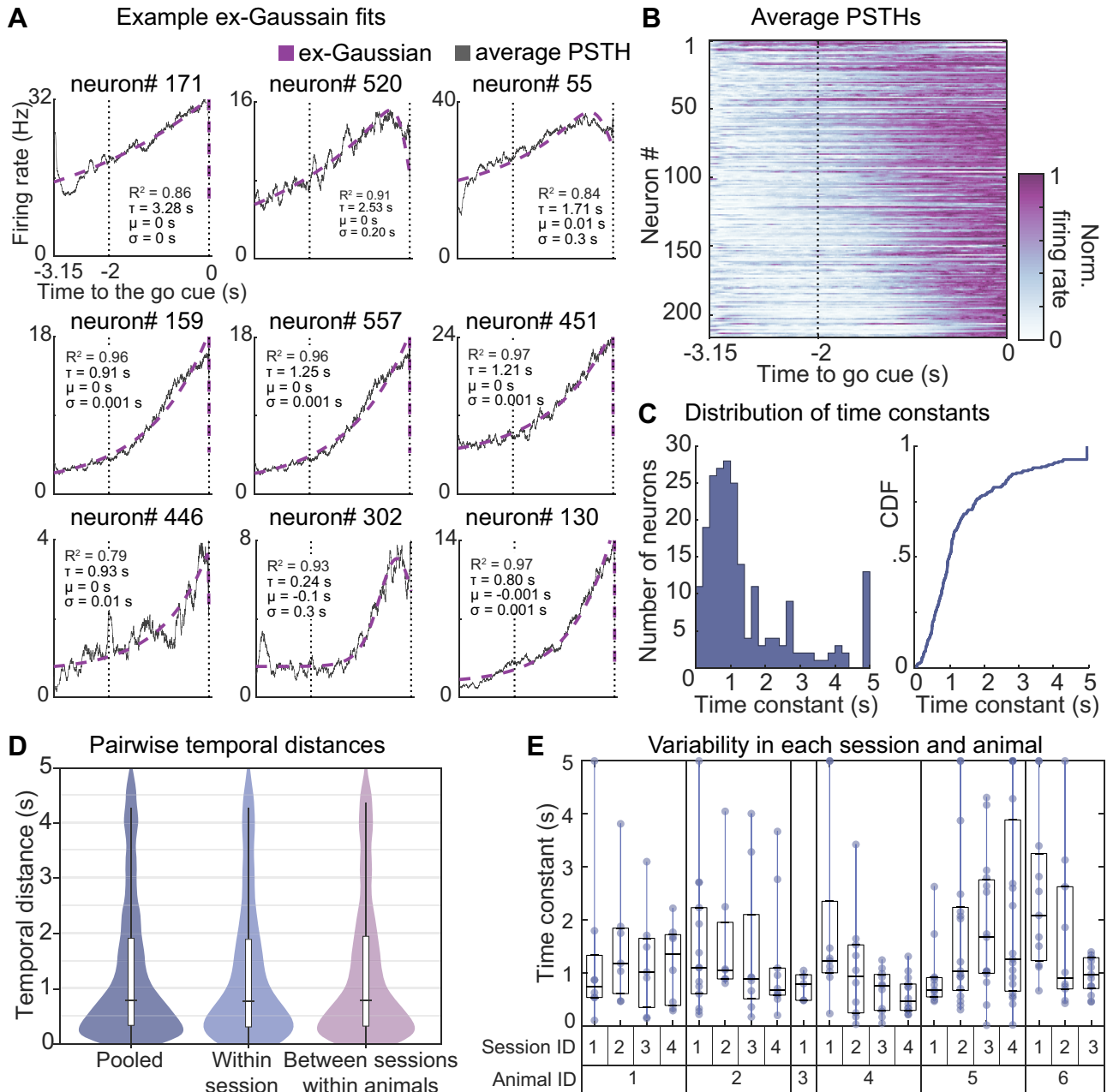
Figure 2. Neuronal firing rates ramp up at various timescales in the ALM cortex. *A*: ex-Gaussian receptive field model fits for nine example ALM neurons. Firing rates of neurons are depicted as thin black lines. Ex-Gaussian models are depicted as dashed purple lines. *B*: heatmap of normalized firing rates across 216 ALM neurons. Each row represents the averaged normalized firing rate for a single neuron. Neurons were sorted by their estimated value of τ, from larger τ or longer time constant to smaller τ or shorter time constant. *C*: histogram and cumulative distribution of estimated time constants. On the left is a histogram of the marginal distribution of the τ values. On the right is the cumulative distribution function (CDF) of τ in purple solid line. *D*: violin plots of pairwise temporal distances were calculated between neurons from all recording sessions and animals (*left*), the same session (*middle*), and different sessions of the same animals (*right*). Temporal distance was measured as the absolute difference between time constant (τ) values. *E*: box plots representing the variability of time constants (τ) for ALM neurons within individual sessions and across different animals. Estimated τ values varied among neurons in each recording session, with some variability across sessions and minimal variability across animals. ALM, anterior lateral motor.

greater number of neurons showed longer time constants than would be expected under a normal distribution. A similarly wide range of time constant values was obtained using an alternative autocorrelation-based approach (23) for estimating neuronal time constants (Supplemental Fig. S1). In contrast to the wide range of ramping time constants, there was relatively little variability in peak response times ($\mu = 0$ s in 90% of the 216 neurons). These patterns closely resemble

the temporally diverse responses of neurons in the monkey (7) and rodent (6) entorhinal cortex.

As neurons were pooled across animals and recording sessions, we wanted to determine whether the temporal heterogeneity we observed may have reflected unaccounted differences between animals or recording sessions. We measured the temporal distances between pairs of neurons in three distinct conditions. In the first condition, pairwise temporal distances were

measured between neurons from any session and animal (median = 0.78 s, interquartile range = 0.33 s to 1.90 s). In the second condition, pairwise distances were calculated between neurons in the same session (median = 0.76 s, interquartile range = 0.30 s to 1.88 s). Lastly, pairwise distances were estimated between neurons from different sessions of the same animal in the last condition (median = 0.79 s, interquartile range = 0.31 s to 1.94 s). As shown in Fig. 2D, pairwise distances were similar across the pooled, intrasession, and intersession conditions. This consistency in pairwise distances indicates that the variability of neuronal time constants within a single recording session is as pronounced as the variability across different sessions.

To further dissect the contributions of session-to-session variability and between-animal differences on the heterogeneity of ramping time constants, we used a generalized linear mixed-effects model with the random effects of sessions nested within animals. Variance component analysis revealed that variability across sessions approximately accounted for 9.39% of the variance in neuronal time constants (95% CI = [4.09%, 16.01%], $P < 0.001$ nonparametric bootstrap), while variability across animals captured around 0.84% of the variance (95% CI = [0%, 5.04%], $P = 0.302$). Figure 2E shows the distribution of time constants across individual sessions and animals. Notably, a considerable proportion of the variance remained after accounting for intersession and interanimal variability (89.77%, 95% CI = [83.45%, 94.68%], $P < 0.001$). These results suggest that the observed heterogeneity in ramping time constants primarily reflects intrinsic differences among ALM neurons, rather than variability attributable to different recording sessions or individual animals.

Neurons with Different Time Constants Convey a Spectrum of Time Horizons

Our analyses revealed a broad range of time constants among individual ALM neurons. We asked whether this heterogeneity may have implications on dynamics at the population level. Given the proposal that ramping activity in the ALM may reflect time estimation related to urgency signals (14), we first evaluated whether the joint activity of the 216 neurons carries latent information about time. We trained a decoder using linear discriminant analysis (LDA) to estimate time throughout the 2 s delay period using the population activity of the 216 neurons. We measured the confidence of the decoder at each 100 ms time bin during the delay interval as the log posterior across the range of possible time estimates. The decoder made predictions that were proximal to the actual time bins with an average error of 0.19 s, resulting in a diagonal band across the decoding matrix in Fig. 3A. A χ^2 goodness of fit test indicated that this pattern was different from a uniform distribution that would result from decoding at chance level, $\chi^2 (992) = 2.142$ and $P < 0.001$. A linear regression of the average decoding error at each time bin yielded a negative slope of 0.057 ± 0.008 (Fig. 3B). These results indicate that the population activity of these ALM neurons conveys information that can be used to decode time with increasing precision as time approaches the Go cue.

Next, we investigated whether the temporal information present in the population activity is dependent on the specific range of time constants among its constituent neurons. Neurons were sorted by their estimated τ value then categorized them into slow-, medium-, and fast-ramping groups (Fig. 3C), each consisting of 72 of the 216 neurons. Neurons in the slow-ramping group have τ values greater than 1.29 s, while neurons in the fast-ramping group have τ values less than 0.74 s. LDA analysis was performed to decode time using the population activity of each group separately, as shown in Fig. 3D. The precision of temporal estimation differed between the three groups during 1 s preceding the go cue [one-way ANOVA test: $F(2, 27) = 48.56$, $P < 0.001$]. Not surprisingly, temporal information was less precise among neurons with the slowest time constant (average decoding error = 0.360 s, SD = 0.048 s) than among the medium-ramping (average decoding error = 0.300 s, SD = 0.028 s) and fast-ramping neurons (average decoding error = 0.197 s, SD = 0.033 s, all Ps < 0.01 with Bonferroni correction). The difference in temporal resolutions as a function of ramping time constant is demonstrated in Fig. 3D as the diagonal of the LDA matrix becomes narrower and darker with faster time constants. Even with this difference, temporal information can be successfully decoded well above chance for all three subpopulations [$\chi^2(992) > 63,137$ and all Ps < 0.001]. The results demonstrate that temporal information is present in the population activity of ALM cortex across a wide range of timescales, corresponding to the ramping time constants of its constituent neurons.

Future Movement Direction is Distributed Broadly across Ramping Timescales

The timescale with which neural activity fluctuates can determine how it contributes to different functions. For instance, neurons with longer time constants have previously been shown to be more involved in maintaining items in working memory compared with those with shorter time constants (22, 24). Thus, we evaluated how the temporal heterogeneity relates to the encoding of upcoming movements in the ALM cortex. We first examined the joint distribution of time constants and trial-type selectivity across individual ALM neurons. Selectivity was measured as the normalized difference between the average firing rates estimated at the delay interval for correct right-lick trials and correct left-lick trials, as previously defined in the original report of this dataset (12). Figure 4 shows the marginal distribution of normalized selectivity during the delay interval. As previously reported by Inagaki et al. (12, 17), ALM neurons show a continuous distribution of selectivity with a contralateral bias or right-lick preference (median selectivity = 0.03, interquartile range = −0.14 to 0.30).

A scatterplot of τ as a function of the absolute value of selectivity is shown in Fig. 4B for neurons in the slow-, medium-, and fast-ramping groups. There was no significant correlation between τ and absolute selectivity value (Kendall's $\tau = 0.02$, $P = 0.74$). To evaluate the strength of this null finding, we calculated a Bayes factor ($BF_{01} = 18.05$) for whether neurons with varying time constants exhibit similar levels of trial-type selectivity (null hypothesis) or differ in their selectivity (alternative hypothesis). This value indicates that the data are 18.05 times more likely under the null hypothesis, which suggests that information about the direction of
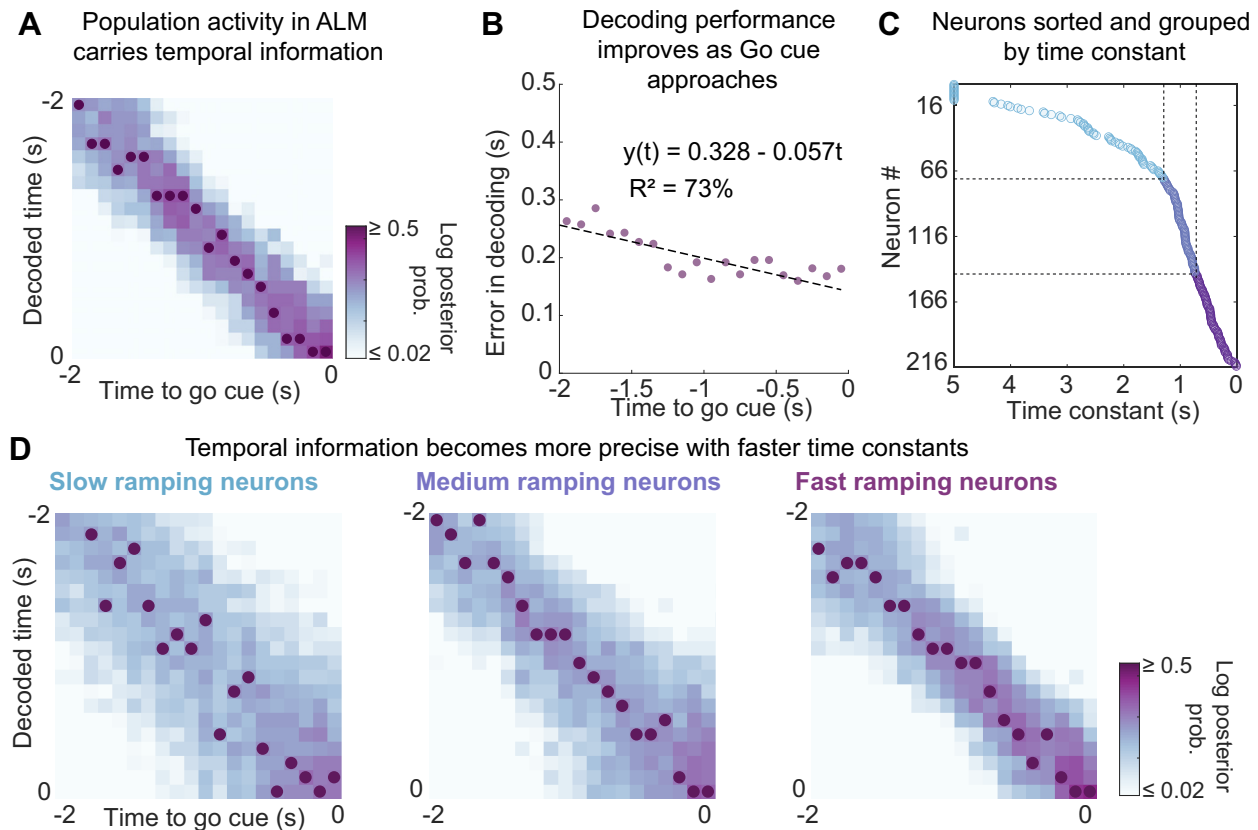
Figure 3. Population activity in the ALM cortex conveys information about time relative to the Go cue. *A*: a linear discrimination analysis (LDA) decoder was trained to classify 100 ms time bins along the 2 s delay interval on the *y*-axis from the population activity of ramping neurons at different 100 ms time bins along the 2 s interval on the *x*-axis. The color gradient corresponds to the log posterior probability (confidence) of the decoder's predictions. Dark purple dots mark the location of the maximum log posterior along the *y*-axis for each time bin on the *x*-axis. *B*: decoding error as a function of time within the delay intervals. The *x*-axis shows the 100 ms time bins that tile the 2 s long intervals preceding the Go cue. The *y*-axis shows the average error between the decoder's predictions and the actual time in seconds. A linear fit of the decoding error is plotted as a dashed line, showing a decrease in decoding error as time reaches the end of the delay interval. *C*: ALM neurons sorted and grouped by τ. The 216 ramping neurons on the *y*-axis were sorted by their estimated time constant τ on the *x*-axis. Neurons were divided into three groups with equal numbers of neurons (*n* = 72 each) corresponding to fast (dark purple dots), medium (light purple dots), and slow (light blue dots) time constants. The values of τ on the boundaries marked by the dashed lines are 0.74 s and 1.29 s. *D*: time decoded from fast-, medium-, and slow-ramping neurons. Three LDA decoders were exclusively trained on the population activity of neurons in the slow, medium, and fast groups. The slow-ramping population yielded a light broad diagonal (*right*). The fast-ramping population yielded a dark narrow diagonal (*left*). ALM, anterior lateral motor.

upcoming movement is conveyed in the ALM across a range of timescales, without a strong dependence on the neurons' time constants.

Next, we assessed how neurons with different time constants contribute to trial-type encoding at the population level. To this end, we used cross-temporal decoding (CTD) to predict the direction of future movement from neural population activity when decoders are trained and tested on all possible pairs of time points within the delay period (19, 21, 22, 25). The results of CTD are displayed in Fig. 4*C* as 2-D accuracy matrices for the slow-, medium-, and fast-ramping groups. Decoding performance for identical training and testing times are depicted in the diagonal of each matrix. These diagonal elements estimate the presence of information in neuronal responses as a function of time. The off-diagonal elements represent accuracy when training and testing was performed in different time points during the delay, thus measuring the similarity in the neural representation of information across different time points.

High accuracy was observed along the diagonal of the accuracy matrix for neurons in the slow-ramping group. This demonstrates that trial-type information is sustained in the population activity of these neurons throughout the entire delay period. In contrast, decoding accuracy for the fast-ramping group was comparatively lower during the early half of the delay, then increased to match the performance levels observed in the slow-ramping group. These results indicate that neurons with different time constants contribute to trial-type selective signals at the population level that emerge with varying latency over the delay period.

Decoding accuracy was uniformly high across the off-diagonal elements for the slow-ramping group, demonstrating a stable representation (26) of trial type that generalizes across different time points in the delay period. Alternatively, off-diagonal accuracy decreased in the fast-ramping group as decoders were trained and tested in distal time points (contours lines in Fig. 4*C*). This decrease in performance implies a dynamic representation (20), whereby activity patterns that distinguish trial conditions gradually evolve at the
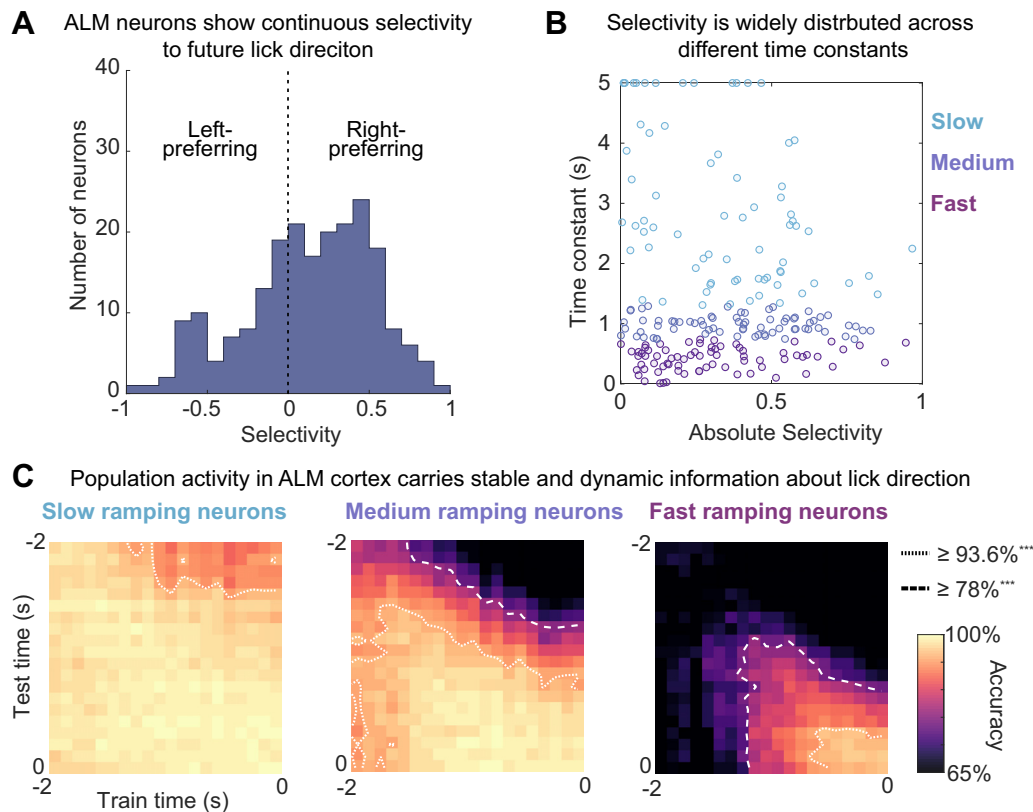
Figure 4. Population activity in the ALM carries stable and dynamic information about trial types. *A*: trial type selectivity is distributed across ALM neurons. A positive selectivity score means firing rate is higher in right-lick than left-lick trials. Negative values indicate the opposite. Values close to zero indicate lack of selectivity. Selectivity was estimated for the delay period of correct trials only. *B*: scatterplot of selectivity and time constants. Information about trial type was distributed broadly across time constants. The *y*-axis shows the absolute value of the normalized selectivity index from *A*. The *x*-axis shows the estimated (τ) values. Each dot represents a neuron colored by their ramping speed. Slow-ramping neurons are light blue dots. Fast-ramping neurons are dark purple dots. Medium-ramping neurons are light purple dots. *C*: accuracy matrices for the cross-temporal decoding (CTD) of trial types using the activity of slow-, medium-, and fast-ramping neurons. LDA classifiers were trained to predict whether animals correctly licked left or right in each trial, at every possible pair of 100 ms time bins along the 2 s delay interval. Each CTC was exclusively trained on the population activity of one group. The color gradient corresponds to decoding accuracy (%). The outermost contour line in each matrix indicates where classifiers performed above chance ($P < 0.001$, one proportion z-test). The interior contour line highlights further significant increases at $P < 0.001$ using two proportion z-tests. Decoding performance for the slow-ramping neurons was consistently high throughout the entire delay interval. Decoding performance for the fast-ramping neurons increased smoothly and peaked around the Go cue. ALM, anterior lateral motor.

population level as time passes during the delay. The contrast in decoding patterns between slow- and fast-ramping neurons suggests that temporal heterogeneity might impact how information about the upcoming movement of the animal might be conveyed to downstream neurons.

Downward Ramping Neurons

As previously reported by Inagaki et al. ([12]), some neurons in the ALM cortex showed a downward ramping of activity from baseline firing rate ($n = 214$ of the 516 delay-active pyramidal neurons). The ex-Gaussian model provided a poorer fit to the firing rates of these neurons (Mean R^2 ± SD = $0.49 ± 0.25$) compared with the upward ramping neurons. Only 55.14% of the downward ramping neurons had an R^2 value greater than 0.5 (Fig. 5*B*), whereas 71.52% of the upward ramping neurons surpassed this criterion. The ramping activity of these neurons showed a more narrow range of time constant values (median = 1.50 s, interquartile range = 1.25 to 1.92 s) than those of upward ramping neurons. Like the upward ramping population, the distribution

of time constant in the downward ramping population was also skewed (skewness = 1.84) and heavy tailed (kurtosis = 6.06). Population-level decoding of time relative to the delay interval indicated that downward ramping activity in the ALM may also carry temporal information at the population-level (average decoding error = 0.264 s, SD = 0.030 s; Fig. 5*D*).

The activity of downward ramping neurons in this brain region has previously been reported to exhibit low levels of selectivity for future movement direction, similar to the activity of local interneurons ([12]). Inagaki et al. ([12]) suggested that downward ramping in the ALM may reflect inhibition by interneurons that integrate inputs from other local pyramidal neurons ([27]). Consistent with this notion, our cross-temporal decoding of trial types indicated that the population-level activity of these downward ramping neurons was less useful than the upward ramping activity for predicting whether an animal will lick rightward or leftward following the delay period (Accuracy range = [50.81–72.58%]; Fig. 5*E*). Together, the results suggest that the diversity of ramping
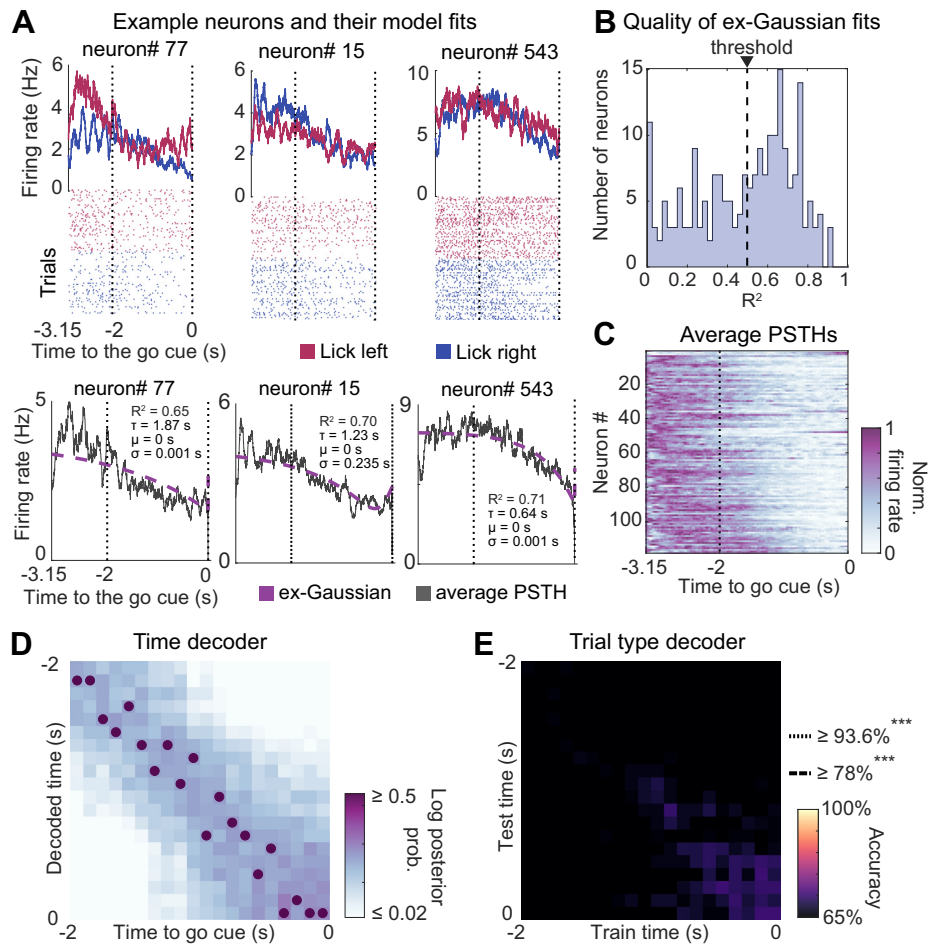
Figure 5. Downward ramping neurons. *A*: firing rate and spike times of three example neurons with downward ramping activity. Blue, low-pitch tone and lick-right. Red, high-pitch tone and lick-left. In the bottom row are the ex-Gaussian model fits. *B*: quality of model fit for downward ramping neurons. A proportion of downward ramping neurons were fit by the ex-Gaussian model above threshold (dashed line). *C*: heatmap of the average PSTHs of downward ramping neurons. *D*: LDA matrix from the decoding of time using the population activity of downward ramping neurons. *E*: cross-temporal decoding of trial type from the population activity of downward ramping neurons. ALM, anterior lateral motor; LDA, linear discrimination analysis.

time constants may be conversed across neural populations in the ALM cortex that vary in their response profiles.

Temporal Heterogeneity Spans across Cortical Depths

Cells in different layers of the cortex can vastly differ in morphological, transcriptomic, and connectivity profiles. In the ALM cortex, two transcriptionally distinct neural populations with nearly identical ramping responses have previously been found in the upper and lower part of layer 5 (16). While information about neuronal types or specific laminar layers were not present in the data we retrieved, Inagaki et al. (12, 17) included the recording depth of each neuron as inferred from manipulator readings. We used this measurement to evaluate whether the temporal heterogeneity we observed across both upward and downward ramping neurons are topologically organized along the cortical depth.

Interestingly, there is strong evidence ($BF_{01} = 19.76$) that variability in ramping time constant do not depend on the depth of recording site (Kendall's $\tau = 0.03$, $P = 0.41$). In contrast, we find that neurons with deeper recording depths show slightly higher degrees of selectivity to future lick direction (Kendall's $\tau = 0.15$, $P < 0.01$), which is consistent with previous reports of strong movement encoding in ALM's deeper layers (28, 29). These analyses were performed across neurons pooled from both the upward and downward ramping population (Supplemental Fig. S2).

DISCUSSION

The heterogeneity of neural dynamics in the ALM cortex is well documented (14, 30–32), but how exactly these dynamics vary across individual neurons has largely remained unexplored. Here, we identified a skewed distribution of ramping time constants across ALM neurons during movement planning, reflecting the diverse speeds at which neuronal firing rates ramped up or down during a delay period preceding the execution of a planned movement (Figs. 1 and 2). We demonstrated that slower ramping activities with longer time constants provided coarse-grained predictions about time relative to the delay, whereas faster ramping activities with shorter time constants offered finer-scale temporal predictions (Fig. 3). Furthermore, we showed that the slower ramping activities provided a stable representation of a movement plan throughout the delay, while the faster ramping ones supported a more dynamic representation that gradually emerged as the delay period neared its end (Fig. 4). Together, these results suggest that the diverse ensemble of ramping dynamics in the ALM may provide a temporal basis set for representing motor plans along a continuum of timescales.

The current results complement other observations of heterogeneous ramping dynamics, characterized by a distribution of time constants, in the medial prefrontal cortex (mPFC) of gerbils during an interval reproduction task (33) and in the entorhinal cortex (EC) of monkeys during the free

viewing of complex images (7). These patterns are consistent with a multiscale representation of time relative to an anticipated future event or a remembered past event. Previous studies have modeled this principle using the Laplace transform (34–37). Just as the Fourier transform decomposes a signal into a set of sinusoidal functions with varying frequencies, the real part of the Laplace transform decomposes a signal into a set of exponential functions with a spectrum of growth or decay rates. For example, the Laplace transform of the time remaining until a target deadline yields exponential curves of the form $e^{-s(T-t)}$ with heterogeneous growth rates s (i.e., the inverse of exponential time constants), resembling the heterogeneous upward ramping activities observed in both the mouse ALM and the gerbil mPFC. In contrast, the Laplace transform of the time elapsed as a past event produces exponential curves with a spectrum of decay rates, mirroring the diverse relaxation rates observed in both the gerbil mPFC and the monkey EC. Our findings add to a growing body of work indicating that the Laplace transform may serve as a general coding scheme in the brain for representing continuous timelines to support efficient and adaptive behavior (6, 7, 33, 38–41).

A signal that evolves monotonically over a set interval inherently holds information about the passage of time, as its progression reflects how much time has elapsed or remains within that interval. By adjusting the speed of that signal, one effectively shifts the timescale at which temporal progression is encoded. Indeed, ramping activity in the primate cortex has been shown to accelerate or decelerate in tasks requiring adaptive adjustments to decision hastiness (42) or movement timing (43). This suggests that a single adjustable ramping signal can offer a sufficient mechanism for flexibly tracking temporal progression across varying timescales. So, what might be the functional implications of temporal heterogeneity within an ensemble of ramping activities?

The diversity of timescales in neural responses across the cortex reflects the time window over which different cortical areas integrate information and contribute to behavioral functions (44–47). Within each area, neurons can vary in their upstream inputs and downstream projections (16, 48), forming a distribution of pathways that support diverse functions operating on different timescales (22, 29, 49–51). Thus, slow-ramping dynamics in the ALM cortex may support the maintenance of an ongoing plan in short-term memory (12, 17), while fast-ramping activities may reflect a dynamic gating mechanism that increases the urgency to commit to the plan as the deadline approaches (14). The graded nature of this variability across neurons may reflect a more fundamental feature of neural systems (52–54). Indeed, continuous variation in neural response patterns appears to be conserved across a wide range of species (55, 56). Such heterogeneity has been suggested to balance efficiency in neuronal encoding with resilience in population dynamics against noise and varying demands (55). One study specifically demonstrated that spiking neural network models with heterogeneous membrane time constants, which follow a heavy-tailed distribution, learn and generalize better across various situations while requiring fewer neurons and synapses than homogeneous networks (57).

The mechanisms responsible for generating and shaping the temporal heterogeneity we observed remain an open question. Evidence from previous studies suggests that molecular heterogeneity, which affects cellular and synaptic processes, can contribute to temporal heterogeneity in neuronal responses. For example, the graded expression of excitatory mGluR1 and inhibitory mGluR2/3 pathways among cerebellar unipolar brush cells has been shown to correlate with continuous variations in their temporal response profiles (58). In the human cortex, gene expression patterns related to transmembrane ion transporters, as well as NMDA and GABA receptors, have been shown to overlap with the gradient of neural timescales estimated from intracranial recordings (59). These findings indicate that molecular mechanisms may shape temporal diversity both within local populations of neurons and more broadly across different cortical areas.

Other studies have proposed network-level mechanisms for generating temporal heterogeneity in neural responses. In network models where units are arranged in a feedforward chain, temporally diverse dynamics have been shown to emerge from a combination of randomness in connection strengths and either a gradient in the strength of local recurrent connections or a gradient in feedforward and feedback connectivity along the chain (60, 61). The incorporation of anatomical constraints into a feedforward chain model further revealed the importance of shorter membrane time constants and steeper gain functions in inhibitory neurons, the gating of long-range excitatory inputs between cortical areas by local inhibition within each area, and the gradient in synaptic excitation across areas (62). More recently, Stern et al. (63) proposed a network model composed of local neuronal assemblies, where larger assemblies display stronger recurrent dynamics that sustain longer-lasting activity. In this model, a lognormal distribution of assembly sizes was shown to generate a heavy-tailed distribution of activity timescales. The presence of recurrent connectivity, along with external ramping inputs, has been shown to be required for a neural network model to replicate the heterogeneous firing rates of ALM neurons and their responses to optogenetic perturbations (14). Together, these past findings point to a gradient in recurrent connectivity as a possible basis for temporally heterogeneous dynamics in the ALM cortex.

The causal contributions of temporal heterogeneity to ongoing network dynamics and behavior remain unknown and are beyond the scope of this study. To address this, future experiments will need to use single-cell resolution perturbations (64). For example, a recent study used an all-optical approach to selectively stimulate hippocampal neurons based on their spatial tuning properties (65). This provided direct evidence for the causal role of place cells in navigation, decades after their initial discovery (66). A similar strategy could be used to selectively target neurons based on their temporal response profiles. Nevertheless, our findings place the ALM cortex on a long list of brain areas that display a skewed distribution of time constants. In the ALM, this diversity spanned neurons with upward- and downward-ramping responses, from different cortical depths, and with varying degrees of selectivity to future lick direction. From the perspective of a downstream neuron, incoming signals from the ALM cortex can provide distinct information about the direction of an upcoming movement and the remaining time until its execution.

DATA AVAILABILITY

The data and basic preprocessing code used in this article was retrieved from an open-source data repository called CRCNS through this URL: https://crcns.org/data-sets/motor-cortex/alm-5/about-alm-5 (12, 17). Basic scripts used for analysis and plotting can be accessed from the GitHub repository: https://github.com/roaffan/temporal-heterogeneity-ramping. The code used for the alternative approach to estimating neural time constant is publicly available as a Python package in this repository: https://github.com/roxana-zeraati/abcTau (23).

SUPPLEMENTAL MATERIAL

Supplemental Figs. S1 and S2: https://doi.org/10.6084/m9.figshare.c.7524384.v1.

DISCLOSURES

M.W.H. is a cofounder of Cognitive Scientific AI, Inc., which can indirectly benefit from the present work. None of the other authors has any conflicts of interest, financial or otherwise, to disclose.

AUTHOR CONTRIBUTIONS

R.O.A. and M.W.H. conceived and designed research; R.A.O., I.M.B., L.N.P., and N.A.C. analyzed data; R.O.A., I.M.B., N.A.C., B.B.S., and M.W.H. interpreted results of experiments; R.O.A. and L.N.P. prepared figures; R.O.A., B.B.S., and M.W.H. drafted manuscript; R.O.A., I.M.B., L.N.P., N.A.C., B.B.S., and M.W.H. edited and revised manuscript; R.O.A., I.M.B., L.N.P., N.A.C., B.B.S., and M.W.H. approved final version of manuscript.

REFERENCES

1. **Jin DZ**, **Fujii N**, **Graybiel AM.** Neural representation of time in cortico-basal ganglia circuits. *Proc Natl Acad Sci USA* 106: 19156–19161, 2009. doi:10.1073/pnas.0909881106.

2. **Cao R**, **Bladon JH**, **Charczynski SJ**, **Hasselmo ME**, **Howard MW.** Internally generated time in the rodent hippocampus is logarithmically compressed. *eLife* 11: e75353, 2022. doi:10.7554/eLife.75353.

3. **MacDonald C**, **Lepage K**, **Eden U**, **Eichenbaum H.** Hippocampal "time cells" bridge the gap in memory for discontiguous events. *Neuron* 71: 737–749, 2011. doi:10.1016/j.neuron.2011.07.012.

4. **Taxidis J**, **Pnevmatikakis EA**, **Dorian CC**, **Mylavarapu AL**, **Arora JS**, **Samadian KD**, **Hoffberg EA**, **Golshani P.** Differential emergence and stability of sensory and temporal representations in context-specific hippocampal sequences. *Neuron* 108: 984–998.e9, 2020. doi:10.1016/j.neuron.2020.08.028.

5. **Tiganj Z**, **Cromer JA**, **Roy JE**, **Miller EK**, **Howard MW.** Compressed timeline of recent experience in monkey lateral prefrontal cortex. *J Cogn Neurosci* 30: 935–950, 2018. doi:10.1162/jocn_a_01273.

6. **Tsao A**, **Sugar J**, **Lu L**, **Wang C**, **Knierim JJ**, **Moser MB**, **Moser EI.** Integrating time from experience in the lateral entorhinal cortex. *Nature* 561: 57–62, 2018. doi:10.1038/s41586-018-0459-6.

7. **Bright IM**, **Meister ML**, **Cruzado NA**, **Tiganj Z**, **Buffalo EA**, **Howard MW.** A temporal record of the past with a spectrum of time constants in the monkey entorhinal cortex. *Proc Natl Acad Sci USA* 117: 20274–20283, 2020. doi:10.1073/pnas.1917197117.

8. **Li N**, **Chen T-W**, **Guo ZV**, **Gerfen CR**, **Svoboda K.** A motor cortex circuit for motor planning and movement. *Nature* 519: 51–56, 2015. doi:10.1038/nature14178.

9. **Zhu J**, **Hasanbegović H**, **Liu LD**, **Gao Z**, **Li N.** Activity map of a cortico-cerebellar loop underlying motor planning. *Nat Neurosci* 26: 1916–1928, 2023. doi:10.1038/s41593-023-01453-x.

10. **Guo ZV**, **Li N**, **Huber D**, **Ophir E**, **Gutnisky D**, **Ting JT**, **Feng G**, **Svoboda K.** Flow of cortical activity underlying a tactile decision in mice. *Neuron* 81: 179–194, 2014. doi:10.1016/j.neuron.2013.10.020.

11. **Li N**, **Daie K**, **Svoboda K**, **Druckmann S.** Robust neuronal dynamics in premotor cortex during motor planning. *Nature* 532: 459–464, 2016. doi:10.1038/nature17643.

12. **Inagaki HK**, **Inagaki M**, **Romani S**, **Svoboda K.** Low-dimensional and monotonic preparatory activity in mouse anterior lateral motor cortex. *J Neurosci* 38: 4163–4185, 2018. doi:10.1523/JNEUROSCI.3152-17.2018.

13. **Inagaki HK**, **Chen S**, **Ridder MC**, **Sah P**, **Li N**, **Yang Z**, **Hasanbegovic H**, **Gao Z**, **Gerfen CR**, **Svoboda K.** A midbrain-thalamus-cortex circuit reorganizes cortical dynamics to initiate movement. *Cell* 185: 1065–1081.e23, 2022. doi:10.1016/j.cell.2022.02.006.

14. **Finkelstein A**, **Fontolan L**, **Economo MN**, **Li N**, **Romani S**, **Svoboda K.** Attractor dynamics gate cortical information flow during decision-making. *Nat Neurosci* 24: 843–850, 2021. doi:10.1038/s41593-021-00840-6.

15. **Birnbaum JE**, **Hasnain MA**, **Nunez JLU**, **Hartman E**, **Chandrasekaran C**, **Economo MN.** Separating cognitive and motor processes in the behaving mouse. *bioRxiv*, 2024. doi:10.1101/2023.08.23.554474.

16. **Economo MN**, **Viswanathan S**, **Tasic B**, **Bas E**, **Winnubst J**, **Menon V**, **Graybuck LT**, **Nguyen TN**, **Smith KA**, **Yao Z**, **Wang L**, **Gerfen CR**, **Chandrashekar J**, **Zeng H**, **Looger LL**, **Svoboda K.** Distinct descending motor cortex pathways and their roles in movement. *Nature* 563: 79–84, 2018. doi:10.1038/s41586-018-0642-9.

17. **Inagaki HK**, **Fontolan L**, **Romani S**, **Svoboda K.** Discrete attractor dynamics underlies persistent activity in the frontal cortex. *Nature* 566: 212–217, 2019. doi:10.1038/s41586-019-0919-7.

18. **Cruzado NA**, **Tiganj Z**, **Brincat SL**, **Miller EK**, **Howard MW.** Conjunctive representation of what and when in monkey hippocampus and lateral prefrontal cortex during an associative memory task. *Hippocampus* 30: 1332–1346, 2020. doi:10.1002/hipo.23282.

19. **King J**, **Dehaene S.** Characterizing the dynamics of mental representations: the temporal generalization method. *Trends Cogn Sci* 18: 203–210, 2014. doi:10.1016/j.tics.2014.01.002.

20. **Meyers E.** Dynamic population coding and its relationship to working memory. *J Neurophysiol* 120: 2260–2268, 2018. doi:10.1152/jn.00225.2018.

21. **Enel P**, **Wallis JD**, **Rich EL.** Stable and dynamic representations of value in the prefrontal cortex. *eLife* 9: e54313, 2020. doi:10.7554/eLife.54313.

22. **Wasmuht D**, **Spaak E**, **Buschman T**, **Miller E**, **Stokes M.** Intrinsic neuronal dynamics predict distinct functional roles during working memory. *Nat Commun* 9: 3499, 2018. doi:10.1038/s41467-018-05961-4.

23. **Zeraati R**, **Engel T**, **Levina A.** A flexible Bayesian framework for unbiased estimation of timescales. *Nat Comput Sci* 2: 193–204, 2022. doi:10.1038/s43588-022-00214-3.

24. **Cavanagh SE**, **Towers JP**, **Wallis JD**, **Hunt LT**, **Kennerley SW.** Reconciling persistent and dynamic hypotheses of working memory coding in prefrontal cortex. *Nat Commun* 9: 3498, 2018. doi:10.1038/s41467-018-05873-3.

25. **Stroud JP**, **Watanabe K**, **Suzuki T**, **Stokes MG**, **Lengyel M.** Optimal information loading into working memory explains dynamic coding in the prefrontal cortex. *Proc Natl Acad Sci USA* 120: e2307991120, 2023. doi:10.1073/pnas.2307991120.

26. **Murray JD**, **Bernacchia A**, **Roy NA**, **Constantinidis C**, **Romo R**, **Wang XJ.** Stable population coding for working memory coexists with heterogeneous neural dynamics in prefrontal cortex. *Proc Natl Acad Sci USA* 114: 394–399, 2017. doi:10.1073/pnas.1619449114.

27. **Kerlin AM**, **Andermann ML**, **Berezovskii VK**, **Reid RC.** Broadly tuned response properties of diverse inhibitory neuron subtypes in mouse visual cortex. *Neuron* 67: 858–871, 2010. doi:10.1016/j.neuron.2010.08.002.

28. **Wang ZA**, **Chen S**, **Liu Y**, **Liu D**, **Svoboda K**, **Li N**, **Druckmann S.** Not everything, not everywhere, not all at once: a study of brain-wide encoding of movement. *bioRxiv*, 2023. doi:10.1101/2023.06.08.544257.

29. **Chen S**, **Liu Y**, **Wang ZA**, **Colonell J**, **Liu LD**, **Hou H**, **Tien N-W**, **Wang T**, **Harris T**, **Druckmann S**, **Li N**, **Svoboda K.** Brain-wide neural activity underlying memory-guided movement. *Cell* 187: 676–691. e16, 2024. doi:10.1016/j.cell.2023.12.035.

30. **Mahrach A**, **Chen G**, **Li N**, **Van Vreeswijk C**, **Hansel D.** Mechanisms underlying the response of mouse cortical networks to optogenetic manipulation. *eLife* 9: e49967, 2020. doi:10.7554/eLife.49967.

31. **Yang W**, **Tipparaju SL**, **Chen G**, **Li N.** Thalamus-driven functional populations in frontal cortex support decision-making. *Nat Neurosci* 25: 1339–1352, 2022. doi:10.1038/s41593-022-01171-w.

32. **Amsalem O**, **Inagaki H**, **Yu J**, **Svoboda K**, **Darshan R.** Sub-threshold neuronal activity and the dynamical regime of cerebral cortex. *Nat Commun* 15: 7958, 2024. doi:10.1038/s41467-024-51390-x.

33. **Cao R**, **Bright IM**, **Howard MW.** Ramping cells in the rodent medial prefrontal cortex encode time to past and future events via real Laplace transform. *Proc Natl Acad Sci USA* 121: e2404169121, 2024. doi:10.1073/pnas.2404169121.

34. **Howard MW**, **Esfahani ZG**, **Le B**, **Sederberg PB.** Learning temporal relationships between symbols with Laplace neural manifolds. *arXiv*, 2024.

35. **Shankar KH**, **Howard MW.** Timing using temporal context. *Brain Res* 1365: 3–17, 2010. doi:10.1016/j.brainres.2010.07.045.

36. **Shankar KH**, **Howard MW.** A scale-invariant internal representation of time. *Neural Comput* 24: 134–193, 2012. doi:10.1162/NECO_a_00212.

37. **Daniels BC**, **Howard MW.** Continuous attractor networks for Laplace neural manifolds. *arXiv*, 2024. doi:10.48550/arXiv.2406.04545.

38. **Atanas AA**, **Kim J**, **Wang Z**, **Bueno E**, **Becker M**, **Kang D**, **Park J**, **Kramer TS**, **Wan FK**, **Baskoylu S**, **Dag U**, **Kalogeropoulou E**, **Gomes MA**, **Estrem C**, **Cohen N**, **Mansinghka VK**, **Flavell SW.** Brain-wide representations of behavior spanning multiple timescales and states in C. elegans. *Cell* 186: 4134–4151.e31, 2023. doi:10.1016/j.cell.2023.07.035.

39. **Momennejad I**, **Howard MW.** Predicting the future with multi-scale successor representations. *bioRxiv*, 2018. doi:10.1101/449470.

40. **Howard MW**, **Hasselmo ME.** Cognitive computation using neural representations of time and space in the Laplace domain. *arXiv*, 2020. doi:10.48550/arXiv.2003.11668.

41. **Tano P**, **Dayan P**, **Pouget A.** A local temporal difference code for distributional reinforcement learning. *Advances in neural information processing systems* 33: 13662–13673, 2020.

42. **Thura D**, **Cisek P.** Modulation of premotor and primary motor cortical activity during volitional adjustments of speed-accuracy trade-offs. *J Neurosci* 36: 938–956, 2016. doi:10.1523/JNEUROSCI.2230-15.2016.

43. **Wang J**, **Narain D**, **Hosseini EA**, **Jazayeri M.** Flexible timing by temporal scaling of cortical responses. *Nat Neurosci* 21: 102–110, 2018. doi:10.1038/s41593-017-0028-6.

44. **Pinto L**, **Tank DW**, **Brody CD.** Multiple timescales of sensory-evidence accumulation across the dorsal cortex. *eLife* 11: e70263, 2022. doi:10.7554/eLife.70263.

45. **Spitmaan M**, **Seo H**, **Lee D**, **Soltani A.** Multiple timescales of neural dynamics and integration of task-relevant signals across cortex. *Proc Natl Acad Sci USA* 117: 22522–22531, 2020. doi:10.1073/pnas.2005993117.

46. **Honey CJ**, **Thesen T**, **Donner TH**, **Silbert LJ**, **Carlson CE**, **Devinsky O**, **Doyle WK**, **Rubin N**, **Heeger DJ**, **Hasson U.** Slow cortical dynamics and the accumulation of information over long timescales. *Neuron* 76: 423–434, 2012 [Erratum in *Neuron* 76: 668, 2012]. doi:10.1016/j.neuron.2012.08.011.

47. **Manea AMG**, **Maisson DJ-N**, **Voloh B**, **Zilverstand A**, **Hayden B**, **Zimmermann J.** Neural timescales reflect behavioral demands in freely moving rhesus macaques. *Nat Commun* 15: 2151, 2024. doi:10.1038/s41467-024-46488-1.

48. **Hwang EJ**, **Link TD**, **Hu YY**, **Lu S**, **Wang EH-J**, **Lilascharoen V**, **Aronson S**, **O'Neil K**, **Lim BK**, **Komiyama T.** Corticostriatal flow of action selection bias. *Neuron* 104: 1126–1140.e6, 2019. doi:10.1016/j.neuron.2019.09.028.

49. **Spaak E**, **Watanabe K**, **Funahashi S**, **Stokes MG.** Stable and dynamic coding for working memory in primate prefrontal cortex. *J Neurosci* 37: 6503–6516, 2017. doi:10.1523/JNEUROSCI.3364-16.2017.

50. **Tseng S-Y**, **Chettih SN**, **Arlt C**, **Barroso-Luque R**, **Harvey CD.** Shared and specialized coding across posterior cortical areas for dynamic navigation decisions. *Neuron* 110: 2484–2502.e16, 2022. doi:10.1016/j.neuron.2022.05.012.

51. **Cavanagh SE**, **Wallis JD**, **Kennerley SW**, **Hunt LT.** Autocorrelation structure at rest predicts value correlates of single neurons during reward-guided choice. *eLife* 5: e18937, 2016. doi:10.7554/eLife.18937.

52. **Marder E**, **Goaillard J-M.** Variability, compensation and homeostasis in neuron and network function. *Nat Rev Neurosci* 7: 563–574, 2006. doi:10.1038/nrn1949.

53. **Hutt A**, **Rich S**, **Valiante TA**, **Lefebvre J.** Intrinsic neural diversity quenches the dynamic volatility of neural networks. *Proc Natl Acad Sci USA* 120: e2218841120, 2023. doi:10.1073/pnas.2218841120.

54. **Habashy KG**, **Evans BD**, **Goodman DFM**, **Bowers JS.** Adapting to time: why nature may have evolved a diverse set of neurons. *PLoS Comput Biol* 20: e1012673, 2024. doi:10.1371/journal.pcbi.1012673.

55. **Munn BR**, **Müller EJ**, **Favre-Bulle I**, **Scott E**, **Lizier JT**, **Breakspear M**, **Shine JM.** Multiscale organization of neuronal activity unifies scale-dependent theories of brain function. *Cell* 187: 7303–7313.e15, 2024. doi:10.1016/j.cell.2024.10.004.

56. **Song M**, **Shin EJ**, **Seo H**, **Soltani A**, **Steinmetz NA**, **Lee D**, **Jung MW**, **Paik S-B.** Hierarchical gradients of multiple timescales in the mammalian forebrain. *Proc Natl Acad Sci USA* 121: e2415695121, 2024. doi:10.1073/pnas.2415695121.

57. **Perez-Nieves N**, **Leung V**, **Dragotti P**, **Goodman D.** Neural heterogeneity promotes robust learning. *Nat Commun* 12: 5791, 2021. doi:10.1038/s41467-021-26022-3.

58. **Guo C**, **Huson V**, **Macosko EZ**, **Regehr WG.** Graded heterogeneity of metabotropic signaling underlies a continuum of cell-intrinsic temporal responses in unipolar brush cells. *Nat Commun* 12: 5491, 2021. doi:10.1038/s41467-021-22893-8.

59. **Gao R**, **van den Brink RL**, **Pfeffer T**, **Voytek B.** Neuronal timescales are functionally dynamic and shaped by cortical microarchitecture. *eLife* 9: e61277, 2020. doi:10.7554/eLife.61277.

60. **Chaudhuri R**, **Bernacchia A**, **Wang X.** A diversity of localized timescales in network activity. *eLife* 3: e01239, 2014. doi:10.7554/eLife.01239.

61. **Chaudhuri R**, **Knoblauch K**, **Gariel M-A**, **Kennedy H**, **Wang X-J.** A large-scale circuit mechanism for hierarchical dynamical processing in the primate cortex. *Neuron* 88: 419–431, 2015. doi:10.1016/j.neuron.2015.09.008.

62. **Li S**, **Wang X-J.** Hierarchical timescales in the neocortex: Mathematical mechanism and biological insights. *Proc Natl Acad Sci USA* 119: e2110274119, 2022. doi:10.1073/pnas.2110274119.

63. **Stern M**, **Istrate N**, **Mazzucato L.** A reservoir of timescales emerges in recurrent circuits with heterogeneous neural assemblies. *eLife* 12: e86552, 2023. doi:10.7554/eLife.86552.

64. **Tong L**, **Han S**, **Xue Y**, **Chen M**, **Chen F**, **Ke W**, **Shu Y**, **Ding N**, **Bewersdorf J**, **Zhou ZJ**, **Yuan P**, **Grutzendler J.** Single cell in vivo optogenetic stimulation by two-photon excitation fluorescence transfer. *iScience* 26: 107857, 2023. doi:10.1016/j.isci.2023.107857.

65. **Robinson NTM**, **Descamps LAL**, **Russell LE**, **Buchholz MO**, **Bicknell BA**, **Antonov GK**, **Lau JYN**, **Nutbrown R**, **Schmidt-Hieber C**, **Häusser M.** Targeted activation of hippocampal place cells drives memory-guided spatial behavior. *Cell* 183: 1586–1599.e10, 2020. doi:10.1016/j.cell.2020.09.061.

66. **O'Keefe J**, **Dostrovsky J.** The hippocampus as a spatial map. Preliminary evidence from unit activity in the freely-moving rat. *Brain Res* 34: 171–175, 1971. doi:10.1016/0006-8993(71)90358-1.